Optical Materials: X 2 (2019) 100030

Contents lists available at ScienceDirect

Optical Materials: X

journal homepage: www.journals.elsevier.com/optical-materials-x

Invited Article

(INVITED) Methods for determining the refractive indices and thermo-optic coefficients of chalcogenide glasses at MIR wavelengths

Y. Fang[a,b], D. Furniss[a], D. Jayasuriya[a,c], H. Parnell[a,d], Z.Q. Tang[a], D. Gibson[e], S. Bayya[e], J. Sanghera[e], A.B. Seddon[a], T.M. Benson[a,*]

[a] Mid-Infrared Photonics Group, George Green Institute for Electromagnetics Research, Faculty of Engineering, University of Nottingham, University Park, NG7 2RD, Nottingham, UK
[b] Now Shenzhen Engineering Laboratory of Phosphorene and Optoelectronics, Collaborative Innovation Center for Optoelectronic Science and Technology, And Key Laboratory of Optoelectronic Devices and Systems of Ministry of Education and Guangdong Province, Shenzhen University, Shenzhen, 518060, People's Republic of China
[c] Now at ThorLabs, 1 St. Thomas Place, Ely, CB7 4EX, UK
[d] Now at Granta Design Ltd. (Materials Intelligence), Rustat House, 62, Clifton Rd, Cambridge, CB1 7EG, UK
[e] Naval Research Laboratory, Washington, DC, 20375, USA

ARTICLE INFO

Keywords:
Refractive index dispersion
Thermo-optic coefficient
Chalcogenide glass

ABSTRACT

Chalcogenide glasses have attracted much attention for the realization of photonic components owing to their outstanding optical properties in the mid-infrared (MIR) region. However, relatively few refractive index dispersion data are presently available for these glasses at MIR wavelengths. This paper presents a mini review of methods we have both used and developed to determine the refractive indices and thermo-optic coefficients of chalcogenide glasses at MIR wavelengths, and is supported by new results. The mini review should be useful to both new and established researchers in the chalcogenide glass field and fields of MIR optics, fiber-optics and waveguides. Three groups of methods are distinguished: (1) spectroscopic ellipsometry, (2) prism-based methods, and (3) methods using Fourier transform infrared (FTIR) transmission data. The mini review is supported by a brief discussion of refractive index models.

1. Introduction

A chalcogenide glass is a glass based on one or more Group 16 elements of the Periodic Table, sulfur (S), selenium (Se), or tellurium (Te), usually formulated with additions of germanium, arsenic or antimony to improve glass stability and robustness [1]. Since chalcogenide glasses provide a wide range of glass compositions, different physical properties can be achieved, including refractive index. The properties of mid-infrared (MIR) transparency, high refractive index, low phonon energy, high optical non-linearity [2], and an ability to dope them with rare-earth element ions [3–7], make chalcogenide glasses attractive candidates for use in planar photonic integrated circuits [8,9], narrow- and broad-band fiber-based luminescence [10–12] and laser sources [13,14] and amplifiers [15–17] operating at MIR wavelengths (3–50 μm). Although much research effort has been paid to the development and characterization of chalcogenide glasses for photonics, relatively few refractive index dispersion and thermo-optic coefficient data are presently available at MIR wavelengths, see for example [18–24] with the notable exception of the few chalcogenide glasses used commercially in optics [25–39].

Refractive index, and frequently its wavelength dispersion, is a key parameter that influences the design of optical components. Techniques and insight into obtaining these data can be found, along with the data for many materials in Ref. [40]. However, many different compositions of chalcogenide glasses have been developed depending on the intended application; the refractive index dispersion behavior of these must be routinely assessed. Recent work includes the development of compositions that include Ga or In solubilizers for rare-earth dopant ions [41,42], compositions in which Sb has replaced As for fiber-based MIR medical sensing applications [43,44], selenide-telluride glasses for longer wavelength operation [45], and glass compositions for both high [14,20] and low numerical aperture step-index fibers yet whose glass transition and viscosity-temperature behavior remain sufficiently matched to allow successful fiber-drawing. In this mini review, we shall present illustrative refractive index dispersion results for some $Ge_{20}Sb_{10}Se_{70}$ atomic % (at. %), $Ge_{20}Sb_{10}Se_{67}S_3$ at. %, $As_{40}Se_{60}$ at. %, rare earth ion doped and un-doped GeAsGaSe (Pr^{3+} doped $Ge_{16}As_{21}Ga_1Se_{62}$ and $Ge_{16.5}As_{16}Ga_3Se_{64.5}$ at. %), $Ge_{16}As_{24}Se_{15.5}Te_{44.5}$

* Corresponding author.
E-mail address: Trevor.benson@nottingham.ac.uk (T.M. Benson).

https://doi.org/10.1016/j.omx.2019.100030
Received 15 June 2019; Accepted 30 July 2019
Available online 29 August 2019

at. % and $As_{39}S_{61}$ at. % compositions. The glass compositions quoted throughout are the nominal batch compositions; SEM-EDX analysis shows that the final glass composition is within a few at. % of the nominally batched compositions for these glasses [43,45]. Techniques commonly used for the refractive index measurement include the modeling of transmission or reflection spectroscopic data [46–49], spectroscopic ellipsometry [18,20,22], prism coupling [19,50], grating coupling [51], and the measurement of the minimum deviation angle of light passing through a prism [24,52]. Several of these techniques require intensive sample preparation, are time consuming, and are costly to conduct. More importantly, it has, until recently, been difficult to apply some of these techniques to the MIR spectral region because of the scarcity of suitable beam sources [49]. However, as shall be shown in Section 4 of this mini review paper, the development of quantum cascade and interband cascade lasers [53,54] provide access to new discrete MIR wavelengths, whilst mid-infrared supercontinuum sources [14] can offer broad bandwidth with sufficient average power over a small (filtered) spectral band for refractive index measurements.

The Swanepoel method [46] for determining the refractive indices and thickness of thin films from wavelength measurements on their transmission spectra was recently modified by us for changing the dispersive model from a Cauchy equation to a two-term Sellmeier equation [23]. This modified method successfully determined the refractive indices of chalcogenide glass thin films over the wavelength range from 2 to 25 μm, with an error of less than 0.4%. This technique, and some subsequent developments of it, are reviewed in Section 4 of this paper. Despite being an important parameter for the design thermal lenses, fiber laser sources and other high-quality photonic devices, the thermo-optic coefficients (change of the real part of refractive index n with temperature T, i.e. dn/dT) of chalcogenide glasses is only occasionally reported [21,22]. In this paper, we review the measurements of thermo-optic coefficients of chalcogenide glasses using both prism minimum deviation angle measurements in Section 4.4 and the transmission spectra of thin films in Section 5.3.

The rest of the paper is organized as follows. Section 2 briefly overviews some common models and data fitting equations used to describe refractive index dispersion, to aid the further discussions. Methods for determining the refractive indices and thermo-optic coefficients of chalcogenide glasses are reviewed in Sections 3-5. Section 3 covers spectroscopic ellipsometry, Section 4 reviews prism-based methods and Section 5 introduces techniques based on the transmission of light through thin films. Finally, some conclusions are drawn in Section 6.

2. Refractive index models and data fitting equations

Many descriptions of material refractive index dispersion exist. Some of these, such as the Cauchy and Sellmeier equations describe only the real part of the refractive index [55] whereas others, such as the Drude [55] and the Tauc-Lorentz models [56,57], consider both the real and imaginary parts of the refractive index. This section provides a brief summary of some widely used dispersive models and fitting equations used for describing and interpolating refractive index dispersion data.

2.1. Cauchy equation

The Cauchy dispersion equation is only valid away from band gaps, where the imaginary part of refractive index is very small and there is normal, not anomalous, dispersion. In other words, the equation is valid in the optically transparent regions [58,59]. The Cauchy equation is:

$$n^2(\lambda) = A_1 + \frac{A_2}{\lambda^2} + \frac{A_3}{\lambda^4} \tag{1}$$

where n is the real part of refractive index and A_1, A_2 and A_3 are fitting parameters.

The description, according to Eq. (1), assumes that the band gap, where a resonance in refractive index occurs, is at zero frequency. Hence, the Cauchy equation cannot be used if the band gap or other electronic or vibrational photon absorption of the material falls within the wavelength range of interest [59].

2.2. Sellmeier equation

The Sellmeier equation, first derived in 1871 [60], is one of the most widely used representations of refractive index dispersion. Like the Cauchy equation, the Sellmeier model is valid away from optical band gaps and other absorption bands, i.e. in the normal dispersion region. However, unlike the Cauchy equation, the Sellmeier equation can be applied to materials with multiple band gaps and other material absorption bands in the frequency range of interest [58]. The Sellmeier equation describes the real part of refractive index n as:

$$n^2(\lambda) = A + \sum_{i=1}^{N_s} \frac{B_i\lambda^2}{\lambda^2 - C_i^2} \tag{2}$$

where A, B_i and C_i are experimentally determined Sellmeier coefficients, and N_s is the number of non-constant Sellmeier coefficients used. In this paper, when $N_s = 1$, the equation in Eq. (2) is referred to as a one-term Sellmeier equation. Similarly, a two-term Sellmeier equation is defined when $N_s = 2$.

Eq. (2) describes multiple material resonances at N_s wavelengths; the relevant term in Eq. (2) then becomes singular when $\lambda = C_i$. A two-term Sellmeier equation, with one resonance located in the ultraviolet (UV) region and the other in the infrared (IR) region, is deemed sufficient for most solid materials, in describing their transmissive window across a wide frequency range away from absorption bands [58]. In agreement with this, a two-term Sellmeier equation, with one resonant visible-region absorption and one resonant mid-infrared absorption, was determined as sufficient and appropriate for fitting the continuous linear refractive index dispersion of two bulk chalcogenide glass compositions over the whole wavelength range for which their respective extinction coefficients were less than 0.0005 in Ref. [59]. This will be explored further in Section 3.2.3 of this paper.

For many optical dielectrics, especially those operating in the infrared where the transparency region can be close to the absorption edge, a Herzberger [61] fit may be more appropriate to describe the refractive index as a function of wavelength. The Herzberger formula is a mixed power series,

$$n(\lambda) = A + \frac{B}{\lambda^2 - 0.028} + \frac{C}{(\lambda^2 - 0.028)^2} + D\lambda^2 + E\lambda^4 + F\lambda^6 \tag{3}$$

where A, B, C, D, E, and F are experimentally determined coefficients and is functionally similar to the Sellmeier formula [62]. The term 0.028 in the denominator corresponds to a high frequency, short wavelength, absorption edge that is suitable for materials operating in the infrared but can further be parametrized if appropriate. Other functionally similar formulae including Conrady, Schott, and variants are sometimes used and are available in commercial optical design software such as Zemax OpticStudio and Synopsis CodeV.

Compared to a two-term Sellmeier fit, the Herzberger fit provided a better fitting performance for some chalcogenide glasses over the wavelength range from 0.7 to 14 μm, despite them being amorphous semiconductors. When the fitting range is close to the infrared fundamental absorption band (above 25 μm), the Herzberger fit performs worse than the two-term Sellmeier fit due to the lack of a resonance in the fit, which is there in reality, located in the infrared region.

2.3. Lorentz models

The Lorentz model is a prototype to model many materials [63]. Once material absorption becomes important the Cauchy and Sellmeier

equations are not accurate. Refinements developed by Jellison and Modine in Refs. [56,57] provide a parameterized model of the dielectric constant (and hence complex refractive index) which is consistent with the Kramers–Kronig (K–K) relationship. This is achieved by combining a Tauc absorption edge [64] with classical oscillator broadening [65]. The resulting Tauc-Lorentz (TL) dispersion formula is typically used for amorphous materials and is reported to be very accurate compared to other refractive index descriptions [56,57]. Another refinement is the Cody-Lorentz (CL) oscillator model [66,67] which uses a Cody absorption edge profile instead of a Tauc one.

3. Spectroscopic ellipsometry (SE)

3.1. Introduction

The continuous linear refractive index dispersion of chalcogenide glasses can be obtained using spectroscopic ellipsometry (SE). SE measures the amplitude and relative phase changes of s- and p-polarized light upon reflection over a range of angles and fits them to a refractive index model. The models considered in the present paper were briefly reviewed in Section 2. SE provides measurement of optical constants of the materials over a wide wavelength range and so has an advantage over the traditional prism measurement and prism coupling techniques discussed in the next section which are limited by the fact that coherent light sources of all wavelengths are not available. The accuracy in measuring the refractive index by means of SE is inherently limited by surface effects [49] as a thin contamination layer, e.g. oxide layer in the case of chalcogenides, or small defects on the surface can all potentially yield different optical constants of the glass. Nevertheless, the spectroscopic ellipsometer is considered by many researchers as an effective tool with which to obtain the refractive index data of a chalcogenide bulk glass [18,20,22,68–70] or thin films [71–76] in the MIR region. Table 1 summarizes some of the recent applications of SE in determining the refractive indices of chalcogenide glasses.

3.2. Chalcogenide glass characterization

3.2.1. Bulk glass characterization

Němec et al. [68] measured the linear refractive index of chalcogenide glasses ($As_{40}Se_{60}$ at. % and $Ge_{28}Sb_{12}Se_{60}$ at. %) using spectroscopic ellipsometry (J A Woollam Co., Inc.). A Cauchy-like dispersion equation was adopted to derive refractive indices in the NIR (near-infrared)-MIR spectral range. The refractive index dispersion data obtained were compared to those obtained from a prism coupling method; the comparison confirmed the reliability of infrared spectroscopic ellipsometry.

In Ref. [20], spectroscopic ellipsometry was used to determine the refractive index dispersion of $As_{40}Se_{60}$ at. % and $Ge_{10}As_{23.4}Se_{66.6}$ at. % glasses in the MIR region using a Sellmeier equation as the refractive index description; this provided a good fit to the refractive index dispersion accurate up to 99.9% with respect to prism minimum deviation measurements taken as the benchmark. Dantanarayana et al. claimed in Ref. [20] that unlike the Cauchy model, which does not encompass the entire transparent window of a chalcogenide glass, a two-term Sellmeier equation, with one resonant VIS (visible) absorption and one resonant IR (infrared) absorption, could effectively describe the refractive index dispersion of a chalcogenide glass across the whole MIR region. Recently, Wang et al. [22] measured the refractive indices and thermo-optic coefficients of $Ge_{14}As_xSe_{86-x}$ (x = 4, 8, 12, 16, 20, 23.2, 28, 32) at. % and $Ge_xAs_{12}Se_{88-x}$ (x = 17, 21, 23.3, 25, 27.5, 29, 33) at. % glasses in the 2 μm–12 μm mid-infrared range, but detailed information regarding the fitting model was not mentioned in the paper. In this study of Wang et al., spectroscopic ellipsometry was reported to yield the refractive index accurate to the 4th decimal place.

3.2.2. Thin film characterization

In 2008, the reversible photo-structural effects and metastable photo-refraction in As_4Se_3 at. Ratio films, deposited by Pulsed Laser Deposition, were investigated using spectroscopic ellipsometry [71]. It was found that an as-deposited film had a maximum refractive index compared with the annealed and photo-irradiated films, and that significant metastable reversible photo-refraction was accompanied by photo-darkening. Later, Todorov et al. [72] investigated the optical properties of thin As–S–Se films deposited by physical vapor deposition. In Ref. [72], $As_xS(Se)_{100-x}$ at. % systems exhibited a maximum refractive index, at λ = 632.8 nm, of 3.155 after irradiation and minimum refractive index of 3.031 before photo-irradiation when the composition was $As_{40}Se_{60}$ at. %. Moreover, a photo-darkening effect was observed when the films were exposed to light irradiation (halogen lamp, Ar lasers (λ = 481 and 514 nm) and He–Ne laser (632.8 nm)) In the past few years, spectroscopic ellipsometry has also been applied to characterize the refractive index [71–77], optical band gap [74] and annealing effect [77] of chalcogenide glass thin films. Table 1 also summarizes the recent application of spectroscopic ellipsometry in the

Table 1
Recent application of spectroscopic ellipsometry (SE) to chalcogenide bulk glasses and chalcogenide glass thin films. Adapted from Ref. [78].

1. Glass composition/at. % (exceptions highlighted)	2. Model	3. Wavelength range	4. Refractive index description	5. Ref.
6. Bulk glass characterization				
7. $Ge_{14}As_xSe_{86-x}$ (x = 4, 8, 12, 16, 20, 23.2, 28, 32) and $Ge_xAs_{12}Se_{88-x}$ (x = 17, 21, 23.3, 25, 27.5, 29, 33)	8. IR-VASE, J A Woollam, Lincoln, NE	9.1 μm–13 μm		11 [22].
12. $Ge_{10}As_xTe_{90-x}$ (x = 20, 30, 40, 50, 60) and $Ge_{20}As_{20}Te_{60}$	13. VASE, J A Woollam, Co., Inc., Lincoln, NE	14.0.3 μm–20 μm	15. Cody-Lorentz, Sellmeier	16 [69].
17. $As_{40}Se_{60}/Ge_{10}As_{23.4}Se_{66.6}$	18. VASE, J. A. Woollam, Lincoln, NE	19.0.4 μm–33 μm	20. Sellmeier	21 [20].
22. $As_2Se_3/Ge_{28}Sb_{12}Se_{60}$	23. VASE/IR-VASE	24.0.3 μm–2.3 μm/1.7 μm–20 μm	25. Cody-Lorentz	26 [51].
27. As_{33} $S_{67-x}Se_x$ 28. (x = 0, 17, 33.5, 50 and 67)	29. VASE J A Woollam Co., Inc	30.0.3 μm–2.3 μm	31. Tauc-Lorentz	32 [70].
33. Thin film characterization				
34. As_4Se_3 at. Ratio	35. VASE, J A Woollam Co., Inc.	36.0.5 μm–2.3 μm	37. -	38 [71].
39. $As_xS(Se)_{100-x}$ at. %	40. LEM-3 M1 SE and Rudolph Research SE type 436	41.481 nm–780 nm	42. -	43 [72].
44. $Ge_{90}Te_{10}$ at. %	45. VASE, J A Woollam Co., Inc.	46.3 μm–12 μm	47. Gaussian	48 [73].
49. Inx $(As_2Se_3)1-x$ 50. (x = 0, 0.01, 0.05)	51. VASE, J A Woollam Co., Inc.	52.1.9 eV–4.5 eV	53. -	54 [74].
55. W doped $Ge_2Sb_2Te_5$ at ratio	56. VASE, J A Woollam Co., Inc.	57.0.3 μm–6.2 μm	58. Tauc-Lorentz and Drude	59 [75].
60. $Ge_5Te_{20}Se_{75}$	61. J A Woollam, M-2000	62.0.245 μm–1.7 μm	63. Cody-Lorentz, Gaussian and Tauc-Lorentz	64 [76].

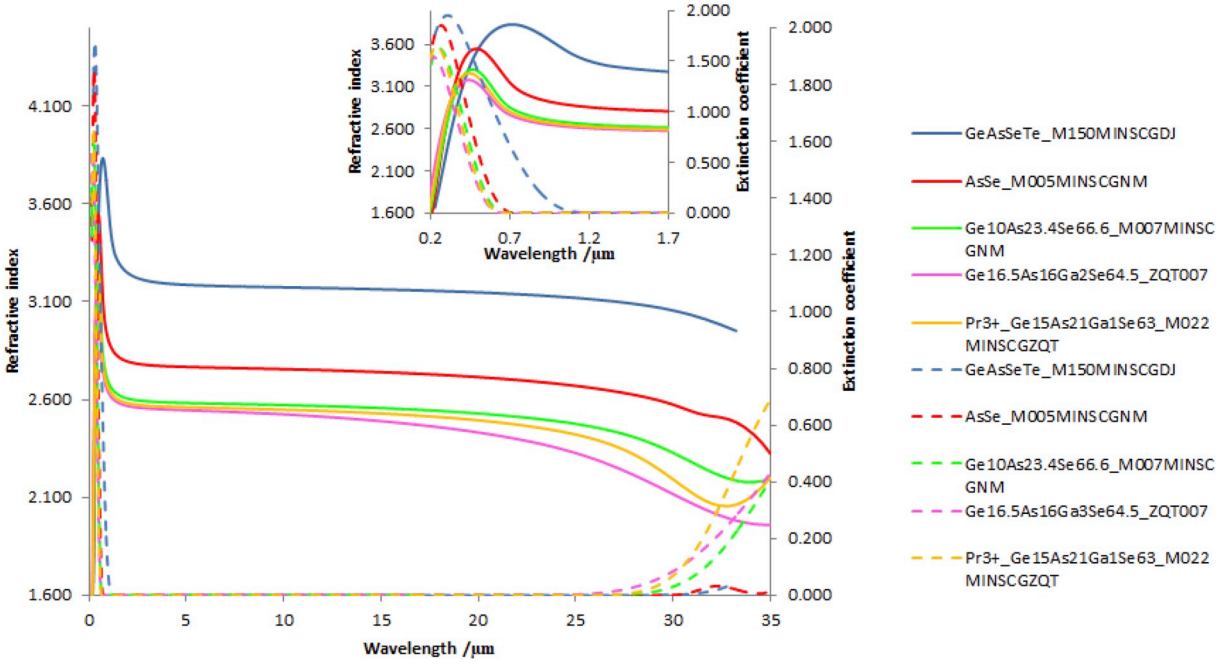

Fig. 1. The refractive indices (solid lines) and extinction coefficients (dashed lines) of $Ge_{16}As_{24}Se_{15.5}Te_{44.5}$, $As_{40}Se_{60}$, $Ge_{10}As_{23.4}Se_{66.6}$, $Ge_{16.5}As_{16}Ga_3Se_{64.5}$ and Pr^{3+} doped $Ge_{16}As_{21}Ga_1Se_{62}$ at. % calculated from ellipsometry measurements. Inset: The refractive indices and extinction coefficients of $Ge_{16}As_{24}Se_{15.5}Te_{44.5}$, $As_{40}Se_{60}$, $Ge_{10}As_{23.4}Se_{66.6}$, $Ge_{16.5}As_{16}Ga_3Se_{64.5}$ and Pr^{3+} doped $Ge_{16}As_{21}Ga_1Se_{62}$ at. % in the 0.2–1.7 μm wavelength range obtained from a Woollam VUV VASE rotating analyzer ellipsometer.

study of chalcogenide bulk glasses and chalcogenide glass thin films.

The refractive indices and extinction coefficients of our bulk $Ge_{16}As_{24}Se_{15.5}Te_{44.5}$, $As_{40}Se_{60}$, $Ge_{10}As_{23.4}Se_{66.6}$, $Ge_{16.5}As_{16}Ga_3Se_{64.5}$ and Pr^{3+} doped $Ge_{16}As_{21}Ga_1Se_{62}$ at. % obtained from the Woollam VUV VASE (measurement range: 140 nm–1700 nm) and IR-VASE (measurement range: 1.7 μm–33 μm) rotating analyzer ellipsometers are shown in Fig. 1 as solid and dashed lines respectively.

Dantanarayana et al. defined the transparent window of a chalcogenide glass to be the range of wavelengths over which the extinction coefficient was smaller than 0.0005 [20]. Therefore, the transparent windows of $Ge_{16}As_{24}Se_{15.5}Te_{44.5}$, $As_{40}Se_{60}$, $Ge_{10}As_{23.4}Se_{66.6}$, $Ge_{16.5}As_{16}Ga_3Se_{64.5}$ and Pr^{3+} doped $Ge_{16}As_{21}Ga_1Se_{62}$ at. % can be determined according to the extinction coefficient plots in Fig. 1. For the $Ge_{16}As_{24}Se_{15.5}Te_{44.5}$ at. % the transparent window is from ~1.44 μm to ~29.46 μm. For the $As_{40}Se_{60}$ and $Ge_{10}As_{23.4}Se_{66.6}$ at. %, the transparent windows are from ~0.7 μm to ~30 μm. The transparent window for $Ge_{16.5}As_{16}Ga_3Se_{64.5}$ at. % is from ~0.65 μm to ~23.5 μm and for Pr^{3+} doped $Ge_{16}As_{21}Ga_1Se_{62}$ at. %, it is from ~0.65 μm to ~26 μm.

3.2.3. Using spectroscopic ellipsometry data to determine appropriate equations for the MIR refractive index dispersion of chalcogenide glasses

In order to find a proper equation to describe the refractive index dispersion of chalcogenide glasses in the MIR region, the two-term Cauchy, three-term Cauchy, one-term Sellmeier, two-term Sellmeier and three-term Sellmeier equations were applied to fit the refractive index data of the chalcogenide glasses (for example: $Ge_{16}As_{24}Se_{15.5}Te_{44.5}$ at. % and $As_{40}Se_{60}$ at. %) in their transparent windows, as shown in Fig. 2. Details of the fitting can be found in Refs. [20,23,24]. The three term Sellmeier equation is referred to as 'three-term Sellmeier (2,1)' when the third term fitted near the optical bandgap electronic absorption and as 'three-term Sellmeier (1,2)' when the third term is allowed in the MIR fundamental vibrational absorption region. The percentage errors in fitting the refractive indices of the $Ge_{16}As_{24}Se_{15.5}Te_{44.5}$ at. % and $As_{40}Se_{60}$ at. % glasses in the MIR region with these equations are shown in Fig. 3(a) and (b). Figs. 2 and 3 reveal that the two-term Cauchy, three-term Cauchy and one-term Sellmeier equations cannot closely describe the refractive index dispersion of $Ge_{16}As_{24}Se_{15.5}Te_{44.5}$ at. % and $As_{40}Se_{60}$ at. % in the MIR regions, with the error larger than 1% for $Ge_{16}As_{24}Se_{15.5}Te_{44.5}$ at. % and larger than 2% for $As_{40}Se_{60}$ at. %. These results confirm that the Cauchy equation should not be used if the band gap falls within the range of interest. Similarly, the one-term Sellmeier equation has only a single resonant Sellmeier term in the NIR region and should not be applied to model materials with multiple band gaps in the frequency range of interest.

Unlike the two-term Cauchy, three-term Cauchy and one-term Sellmeier equations, the two-term Sellmeier equation has one Sellmeier term in the region near the optical bandgap and one in the longer MIR wavelength vibrational overtone and combination region. Therefore, it is suitable to describe the refractive index dispersion of chalcogenide glasses in the MIR regions as shown in Fig. 2(a) and (b). Fig. 3(a) and (b) shows that for both $Ge_{16}As_{24}Se_{15.5}Te_{44.5}$ at. % and $As_{40}Se_{60}$ at. %, the two-term Sellmeier equation can fit the refractive index data well, with an error of less than 0.1%. From Fig. 3, it is also found that the fitting errors are not significantly improved by using the three-term Sellmeier (2,1) equation. Moreover, the fitting error of the three-term Sellmeier (1,2) equation increased from less than 0.1% to less than 0.2% over the wavelength range from 1.5 μm to 30 μm for $Ge_{16}As_{24}Se_{15.5}Te_{44.5}$ at. % and $As_{40}Se_{60}$ at. % compared to the two-term Sellmeier equation. Therefore, the lowest modeling errors were produced by the two-term Sellmeier and three-term Sellmeier (2,1) equations with the error less than 0.1% over the wavelength range from 1.5 μm to 30 μm. Introducing a third Sellmeier term to the two-term Sellmeier equation is shown not to significantly improve the fitting performance, which is in good agreement with the findings of [20].

4. Prism methods

4.1. Basic theory

According to Snell's law, as a beam enters a transparent material from air with an incident angle (less than the critical angle) [66], the

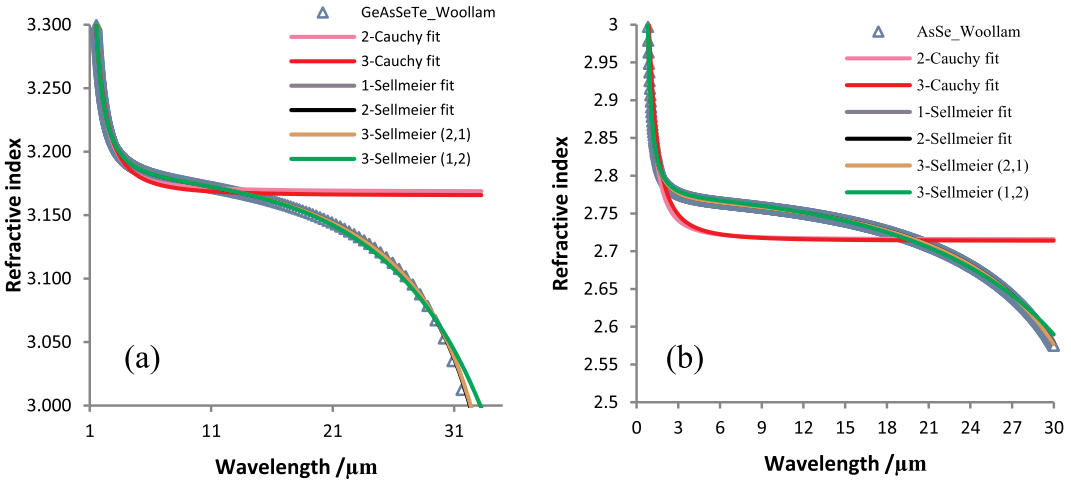

Fig. 2. The fits of the two-term Cauchy, three-term Cauchy, one-term Sellmeier, two-term Sellmeier, three-term Sellmeier (2,1) and three-term Sellmeier (1,2) equations to the refractive index data of the (a) $Ge_{16}As_{24}Se_{15.5}Te_{44.5}$ at. % and (b) $As_{40}Se_{60}$ at. % glasses in the MIR region.

beam is deflected, based on the incident angle and the material's refractive index. A beam traveling through a prism is arranged to be deflected twice: once entering, and again when exiting (See Fig. 4(a)). The deviation angle is defined as the sum of these two deflections as shown in Fig. 4(a).

When a laser beam travels through a prism with a certain incident angle, the minimum deviation position will be achieved as shown in Fig. 4(b), which makes the sum of the two deflections a minimum. Applying Snell's law, and using geometric optics, an expression for the real refractive index n can be obtained as [66]:

$$n = \frac{\sin[(\alpha + \theta)/2]}{\sin(\alpha/2)} \quad (4)$$

where α is the apex angle of prism, and θ is the minimum deviation angle (see Fig. 4).

Another technique for refractive index characterization is prism coupling. The prism coupling technique has been utilized to measure the refractive index in the NIR and MIR spectral regions of chalcogenide glasses in bulk and thin film form. The prism coupling technique essentially measures a laser beam reflected off a prism base which is in as close contact as possible (clamped) with the sample to be measured. The refractive index of the prism material is chosen to be higher than that of the analyte glass. For the bulk material characterization, the refractive index is determined by measuring the critical angle at which total internal reflection occurs at the interface between the prism and sample. For the thin film characterization, the laser beam tunnels across

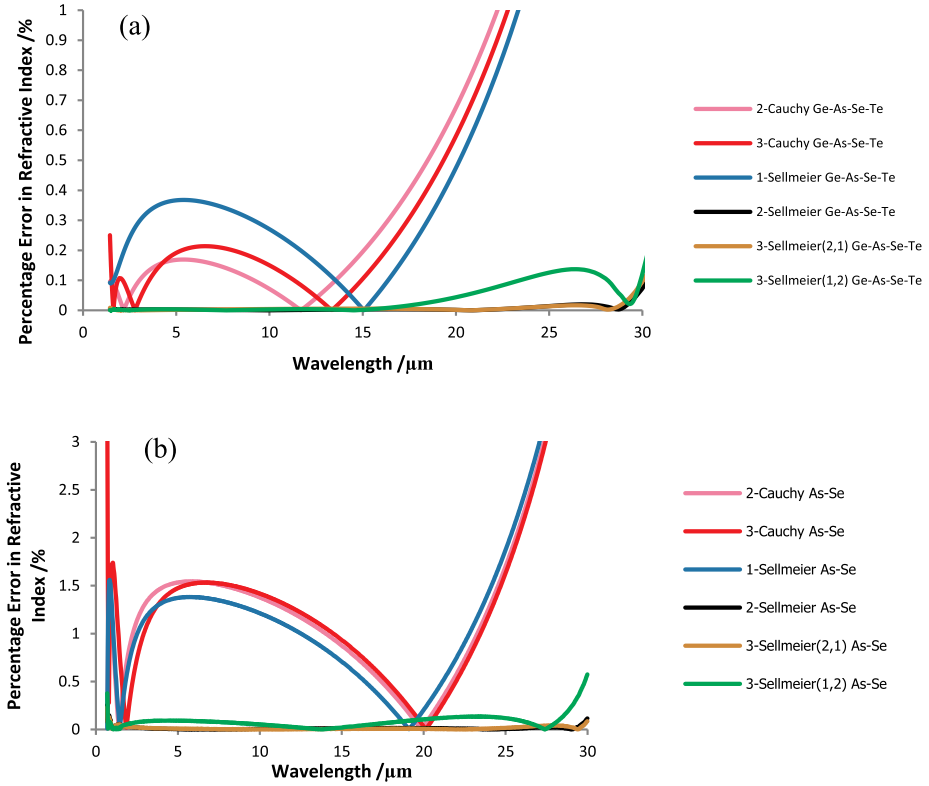

Fig. 3. The percentage errors in fitting the refractive index of the (a) $Ge_{16}As_{24}Se_{15.5}Te_{44.5}$ at. % and (b) $As_{40}Se_{60}$ at. % glasses in the MIR region with the two-term Cauchy, three-term Cauchy, one-term Sellmeier, two-term Sellmeier, three-term Sellmeier (2,1) and three-term Sellmeier (1,2) equations.

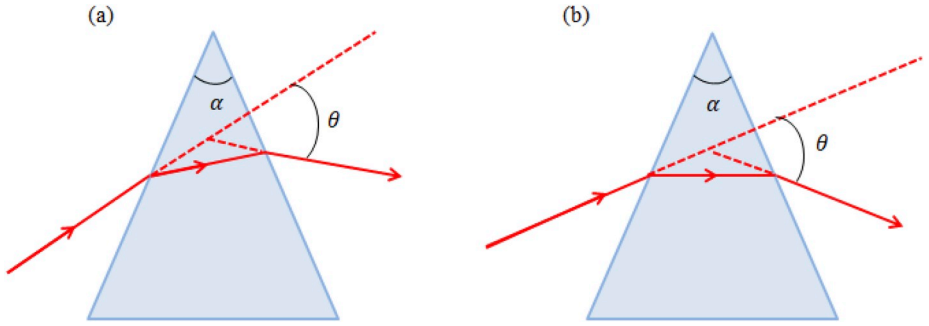

Fig. 4. Schematic diagram showing: (a) the deflections of a beam entering and leaving a prism with an apex angle of α; (b) the minimum deviation position for a beam incident with a certain angle; the sum of the two deflections is a minimum.

any residual air gap between the prism and the film at certain discrete values of the incident angles to become a guided optical propagation mode within the thin film; this is accompanied by a drop in the intensity of light at each coupling angle. The refractive index of a thin film can be obtained by analyzing the locations of the intensity dips and the width between the dips.

4.2. Experimental setup for the minimum deviation measurement at the University of Nottingham, UK

The experimental setup used in the University of Nottingham, UK, is illustrated in Fig. 5. The major components of the apparatus used for the minimum deviation measurement incorporated a laser source (a 651 nm He–Ne class I laser, < 400 μW) coupled with the Agilent fiber coupled diode (1465–1575 nm 40 mW), other MIR beam sources (3.1 μm interband-cascade laser (ICL) from NRL [53,54], SuperK mid-infrared supercontinuum source (1.1–4.2 μm, 450 mW) from NKT Photonics, used in conjunction with a band pass filter (center wavelength: 3.8 μm; FWHM (full width half maximum): 180 nm), or 6.45 μm optical parametric oscillator (OPO) (Chromacity Spark FIR, Chromacity Ltd)), a 1550 nm fiber collimator (model: F230FC-1550, Thorlabs) used for collimating the 651 nm laser source and the 1465–1575 nm tunable laser (see Fig. 5), a prism table with a prism holder on it (E. R. Watts & Son. Ltd. No. 50336), and a plane mirror (Diameter: 48 mm) mounted on the rotation Table 2 as shown in Fig. 5. A screen with an aperture (diameter: ~3 mm) was placed in front of the beam source. When using the visible beam source, a white paper with an aperture (diameter: ~3 mm) in its center was used as the screen. The optical components were mounted on an optical bench (Supplier: Ealing, Size: 178 cm L* 90 cm W*10 cm H) by screws (size: M6). The plane mirror was connected to the rotation Table 2 and the chalcogenide glass prism was mounted on the rotation Table 1, as shown in Fig. 5. The surface of the prism, which was at the rotation center of the rotation table, is defined as surface 1. The other surface of the prism is called surface 2.

Before the minimum deviation measurements, all lasers used in the measurements were aligned to be parallel to the optical bench. Then the plane mirror was adjusted to let the required beam reflect along its own optical path and the position of the plane mirror could be read out from the scope (see Fig. 5) to an accuracy of 5 s. This reading was recorded as zero position reading θ_2', which was used later for calculating the minimum deviation angle.

The prism was placed on the holder and secured using Plasticine©. Then the rotation Table 1 was rotated to find the angles at which each of surface 1 and surface 2, of the chalcogenide glass prism, reflected the beam back along its optical own path. These two readings were recorded as α_1 and α_2, respectively and were used to obtain the apex angle of the measured prism.

After that, the rotation Table 1 was rotated continuously in the same clockwise direction. The light ray was observed to rotate in the same direction as the prism up to a certain point, at which the light beam would change its direction of travel. This position was the minimum deviation position. The plane mirror was adjusted to reflect the beam

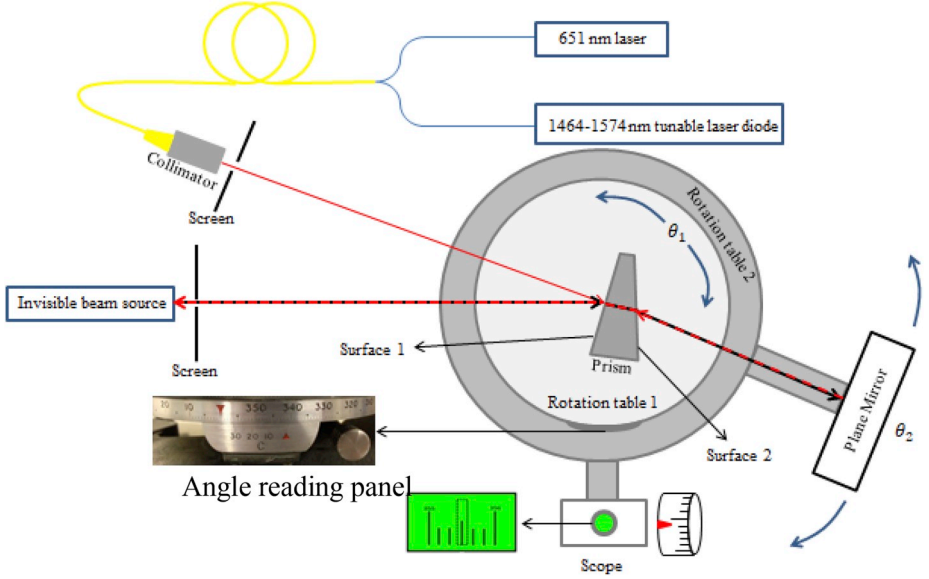

Fig. 5. Schematic diagram of experimental setup for measuring refractive index using minimum deviation method. The chalcogenide glass prism was mounted on the rotation Table 1 and the mirror was connected to the rotation Table 2.

Table 2
The measured apex angle and the values of the refractive indices of the $Ge_{16}As_{24}Se_{15.5}Te_{44.5}$ at. % and $As_{40}Se_{60}$ at. % prisms, together with the standard deviations (s.d.).

65. Wavelength/nm	66. Apex angle (GeAsSeTe)	67. RI (GeAsSeTe)	68. s.d.	69. Apex angle (AsSe)	70. RI (AsSe)	71. s.d.
72.1504	73.10° 16′	74.3.2933	75.0.0012	76.10° 15′	77.2.8404	78.0.0013
79.3100	80.10° 16′	81.3.1920	82.0.0023	83.10° 13′	84.2.8006	85.0.0020
86.3800	87.10° 16′	88.3.1820	89.0.0010	90.10° 14′	91.2.7952	92.0.0010
93.6450	94.10° 16′	95.3.1682	96.0.0010	97.10° 14′	98.2.7863	99.0.0010

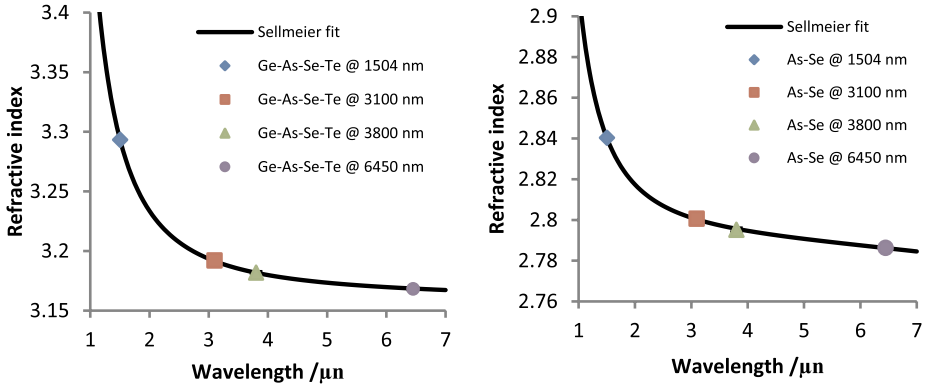

Fig. 6. The refractive indices at wavelengths of 1500 nm, 3100 nm, 3800 nm and 6450 nm with the best two-term Sellmeier fits for the: (a) $Ge_{16}As_{24}Se_{15.5}Te_{44.5}$ at. % and (b) $As_{40}Se_{60}$ at. % prisms.

along its own optical path and the reading of the rotation Table 2 was written down as θ_2''.

The minimum deviation angle was then: $\theta = |\theta_2'' - \theta_2'|$. The refractive index was calculated using Eq. (4). The results of the measurements will be presented and discussed in the following sub-sections.

4.3. Refractive index determination

The minimum deviation method has been proven to be able to determine the refractive index of materials in the range from 1.3 to 2.0 with an accuracy of 1×10^{-6} [79–81], and with the accuracy of measurement of both α and $\theta < 1$". This technique has proved to be suitable for measuring the refractive index of PbTe [82], PbSe [82], GeAsSe [83,84], GeAsS [85], GaGeSbSe [86], $As_{40}Se_{60}$ at. % [23,24], and $Ge_{16}As_{24}Se_{15.5}Te_{44.5}$ at. % [23,24] compositions at certain wavelengths. For example, Zhang et al. used the minimum deviation method to determine the refractive indices of $Ge_{22}As_{20}Se_{58}$ and $Ge_{20}Sb_{15}Se_{65}$ at. %, which were measured at ambient temperature to be 2.4944 and 2.5842 at a wavelength of 10.0 μm, respectively, with an error of ± 0.00015 [83].

Based on the minimum deviation method, a commercial M^3 minimum deviation refractometer (M^3 Measurement System, Inc.) was developed to measure the refractive index of a chalcogenide glass at MIR wavelengths [87–89]. For instance, Novak et al. utilized the M^3 minimum deviation refractometer to obtain the refractive index of $As_{40}Se_{60}$ at. % at wavelengths of 2, 4, 6, 8, 10 and 12 μm before, and after, a thermal molding [89]. This technique is claimed to yield refractive index results accurate to the fourth decimal place at room temperature, if the prism has a sufficiently flat surface.

Carlie et al. modified a commercial system prism coupling system (Metricon model 2010) using additional laser sources, detectors, and a GaP prism in order to enable the measurement of refractive index dispersion at spot wavelengths over the 1.5–10.6 μm range and used it to determine the refractive index of $As_{40}Se_{60}$ at. % bulk glass and thin films across this wavelength region to an accuracy of ± 0.001 [50]. The Authors compared the refractive indices of as deposited and annealed $As_{40}Se_{60}$ at. % films with those of the parent bulk glasses. This work reinforced a theme suggested from the earliest prism-based measurements of the refractive index of arsenic trisulfide ($As_{40}S_{60}$ at. %), for selected wavelengths in the range 0.57–11.8 μm and at three temperatures different samples, which showed that different samples of nominally the same glass composition can have different refractive indices [90]. In bulk samples these differences might arise from a different thermal history (e.g. different quenching or annealing procedures) and unintended compositional differences (e.g. reproducibility of the melt). Subsequent work by Gleason et al. used the modified Metricon prism coupler to investigate the impact of glass composition, and in particular molecular structure, on refractive index and thermo-optic coefficient at a single wavelength of 4.515 μm; they used an optical parametric amplifier (OPA) source and an undoped single crystal germanium prism [21].

In our work, chalcogenide glass prisms ($As_{40}Se_{60}$ at. % and $Ge_{16}As_{24}Se_{15.5}Te_{44.5}$ at. %) were fabricated with a nominal apex angle of 10° using a traditional grinding and polishing technique; the details of the sample preparation are described in Refs. [24,52]. Using the setup with different beam sources, as schematically shown in Fig. 5, the refractive indices of the $Ge_{16}As_{24}Se_{15.5}Te_{44.5}$ at. % and $As_{40}Se_{60}$ at. % glass prisms at a range of NIR and MIR wavelengths are shown in Fig. 6(a) and (b), respectively. The measured apex angles, and the values of the refractive indices of $Ge_{16}As_{24}Se_{15.5}Te_{44.5}$ at. % and $As_{40}Se_{60}$ at. % at certain wavelengths, together with their standard deviations (s.d.), are listed in Table 2.

When measuring the refractive indices of the $Ge_{16}As_{24}Se_{15.5}Te_{44.5}$ at. % and $As_{40}Se_{60}$ at. % prisms using the tunable laser diode, the refractive indices at a wavelength of 1504 nm can be determined with a standard deviation of < 0.0013 as shown in Table 2. When using the ICL (at a wavelength of 3100 nm) for the minimum deviation measurement, the standard deviation of the results for both prisms are < 0.0023, as shown in Table 2. The larger standard deviation is attributed to the poorer beam quality of the ICL compared to that of the well-collimated fiber-coupled tunable laser. Since the beams were well collimated for the SuperK continuum source, used in conjunction with a 3.8 μm band pass filter, and OPO (at a wavelength of 6450 nm), the standard deviations of precision (less than 0.0010) are less than those obtained using the ICL (at a wavelength of 3100 nm). The successful prism measurements using the SuperK continuum source, used in

Table 3
The Sellmeier coefficients (see eqn. (2)) for the refractive indices of the $Ge_{16}As_{24}Se_{15.5}Te_{44.5}$ at. % and $As_{40}Se_{60}$ at. % prisms. R^2 is the coefficient of determination.

100. Sellmeier coefficients	101. a	102. b	103. c	104. a_1	105. a_2	106. R^2
107. As–Se	108.4.062	109.3.726	110.3.244	111.0.3979	112.58.92	113.0.9999
114. Ge-As-Se-Te	115.3.332	116.6.676	117.0.9153	118.0.5022	119.64.37	120.0.9998

conjunction with a 3.8 μm band pass filter, demonstrate the principle that the refractive index at multiple wavelengths in the MIR region can be obtained using the broad band supercontinuum source with band pass filters at different wavelengths.

In order to predict the refractive index at arbitrary wavelengths within the wavelength range over 1500 nm–6450 nm, the data points shown in Fig. 6 were fitted to a two-term Sellmeier equation, yielding the Sellmeier coefficients presented in Table 3. The coefficients of determination, R^2, are over 0.9998 for $Ge_{16}As_{24}Se_{15.5}Te_{44.5}$ at. % and $As_{40}Se_{60}$ at. %; this further confirms that the two-term Sellmeier equation is an effective refractive index description for fitting the refractive index of chalcogenide glasses in the MIR region.

4.4. Thermo-optic coefficient determination

The variation in the index of refraction of a chalcogenide glass with a change in temperature is described as thermo-optic behavior. The refractive index change with temperature in the MIR region is attributed to the thermal excitation of phonons (and electrons in some cases) and can be either positive or negative in sign depending on the composition of the glass. A positive refractive index change in response to an applied thermal load is responsible for phenomena such as thermal lensing, self-focusing and laser damage (at high intensities), and spectral instabilities in laser resonators [91]. Furthermore, in supercontinuum generation (SCG) chalcogenide glass fibers, this refractive index change with temperature is likely to change the confinement of a step-index fiber (SIF) and material dispersion. Despite its importance, few *dn/dT* data are available for chalcogenide glasses in the MIR region [21,22,24], and it is an often overlooked aspect of optical design [92] In Ref. [21], the thermo-optic coefficients of seventeen glasses in the Ge-As-Se glass system were measured at a wavelength of 4.515 μm by means of a prism coupler with an error of ± 11.2 ppm/°C. A simplified thermal version of the Lorentz-Lorenz formula was used to describe the thermo-optic coefficients of the glasses, indicating that the thermo-optic coefficient was related to the thermal polarizability coefficient and the thermal expansion coefficient, following earlier work of Prod'homme [93] and Hilton and Jones [94]. Wang et al. continued the *dn/dT* study of the Ge-As-Se glass system [22]. Thermo-optic coefficients of $Ge_{14}As_xSe_{86-x}$ and $Ge_xAs_{12}Se_{88-x}$ at. % at the wavelength of 10 μm were presented using spectroscopic ellipsometry with an error of ± 6 ppm/°C.

The thermo-optic coefficient (*dn/dT*) can be measured with the minimum deviation setup (described in section 4.2) used in conjunction with an in-house built thermally controlled prism holder, the details of which can be found in Ref. [24]. A simple linearized expression of *dn/dT* follows:

$$\frac{dn}{dT} = \frac{n_h - n_l}{T_h - T_l} \tag{5}$$

where n_h is the refractive index at a higher temperature T_h and n_l is the refractive index at a lower temperature T_l.

The refractive index of an $As_{40}Se_{60}$ at. % prism measured at wavelengths of 1494, 1524 and 1554 nm at different temperatures is presented in Fig. 7(a). It is found that the refractive index decreases with increasing wavelength at each temperature, which agrees with the behavior of the refractive index dispersion of the chalcogenide glass over the temperature range from 20 to 100 °C [22]. The error bar shown for each data point indicates the standard deviation error. Due to the small Δn over the temperature of 16–70.4 °C, a linear fit applied to the data provides a coefficient of determination R^2 of better than 0.9770. The thermo-optic coefficient (*dn/dT*) can be directly obtained as the slope of the linear fits, which are shown in Fig. 7(a) and (b). The measured thermo-optic coefficient of $As_{40}Se_{60}$ at. % is in a good agreement with literature [26] and exhibited a measurement precision error of ± 15.6 ppm/°C. The refractive index of the $As_{40}Se_{60}$ at. % prism measured at a wavelength of 3100 nm at different temperatures is shown in Fig. 7(b). The error bar shown for each data point indicates the standard deviation error, which is 0.001. A linear fit to the data points in Fig. 7(b) yields the value of *dn/dT* as 20.2 ppm/°C with a R^2 of 0.9969. The error of the measured *dn/dT* at this wavelength is within ± 26.0 ppm/°C. As discussed in section 4.3, the error in determining the refractive index of the chalcogenide glasses is larger at this wavelength that that at wavelengths around 1500 nm due to the poorer beam quality of the ICL source used. Fig. 7(a) and (b) show that $As_{40}Se_{60}$ at. % effectively exhibits a linear change in refractive index with temperature over the measurement range at the wavelengths of 1494, 1524, 1554 nm and 3100 nm.

The refractive index of the $Ge_{16}As_{24}Se_{15.5}Te_{44.5}$ at. % prism measured at 1494, 1524 and 1554 nm at different temperatures is presented in Fig. 8(a). The error bar shown for each data point indicates the standard deviation error, which is 0.001. Linear fits were used to fit the data points with an R^2 of better than 0.9905. However, when a quadratic fit was applied to fit the data points, the refractive index variation with temperature was suggested to be nonlinear with the R^2 improved from 0.9905 to 0.9979 as shown in Fig. 8(a). For $Ge_{16}As_{24}Se_{15.5}Te_{44.5}$ at. %, the optical bandgap occurs at longer wavelengths compared to that of $As_{40}Se_{60}$ at. %. It can be seen from the absorbance versus wavelength plot of Fig. 9 that the measurement region here (1494 nm–1554 nm) locates at the standard Urbach edge in the short wavelength cutoff region [24]. From Fig. 9, the optical bandgap of $Ge_{16}As_{24}Se_{15.5}Te_{44.5}$ at. % will shift to longer wavelengths with increasing temperature. Therefore, the suggested nonlinear behavior of *dn/dT* of $Ge_{16}As_{24}Se_{15.5}Te_{44.5}$ at. % in this temperature measurement range is not only attributed to the thermal excitation of phonons, but also to the red shift of optical bandgap with temperature. To fit the increase of the refractive index of $Ge_{16}As_{24}Se_{15.5}Te_{44.5}$ at. % with temperature in this region, a quadratic fit is confirmed to be effective as shown in Fig. 8(a). The *dn/dT* of $Ge_{16}As_{24}Se_{15.5}Te_{44.5}$ at. % at each temperature could be determined with a measurement precision error of ± 15.4 ppm/°C. The refractive index of the $Ge_{16}As_{24}Se_{15.5}Te_{44.5}$ at. % prism measured at a wavelength of 3100 nm at different temperatures is shown in Fig. 8(b) with a standard deviation error of 0.001. Since this measurement wavelength locates beyond the standard Urbach edge, a linear fit proved sufficient to fit the data points with a R^2 of 0.9976 yielding the *dn/dT* at this wavelength to be 213.0 ppm/°C with a measurement precision error of ± 25.6 ppm/°C, as shown in Fig. 8(b).

5. Determining the refractive index and thermo-optic coefficients of chalcogenide glasses using FTIR (Fourier transform infrared) transmission data

5.1. Refractive index determination using FTIR transmission data (improved Swanepoel method)

A method provided by Swanepoel in 1985 [46] allowed the dispersive refractive index and thickness of an amorphous Si:H thin film in

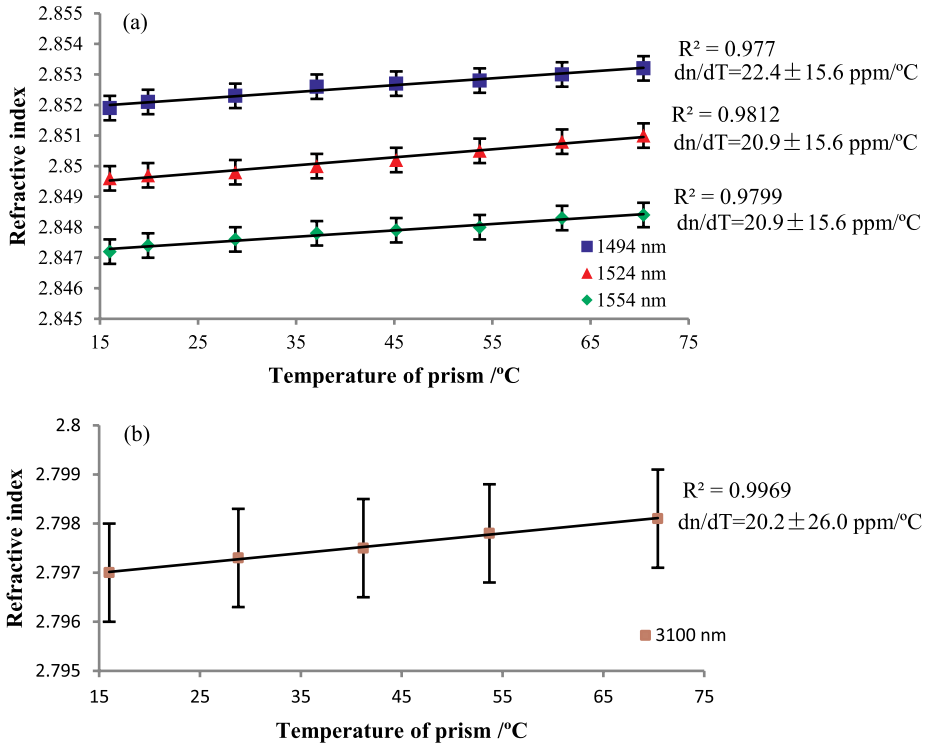

Fig. 7. The refractive index of $As_{40}Se_{60}$ at. % prism varies with temperature at the wavelength of: (a) 1494 nm, 1524 nm, 1554 nm and (b) 3100 nm. Linear fits were applied to the data points.

the transparent region to be determined using only wavelength measurements. The method required measurement at the wavelengths at which maxima and minima occur in two transmission spectra, one taken at normal incidence and another at oblique incidence. This well-known method was later successfully applied by Corrales et al. [95] to determine the refractive index and thickness of the thermally

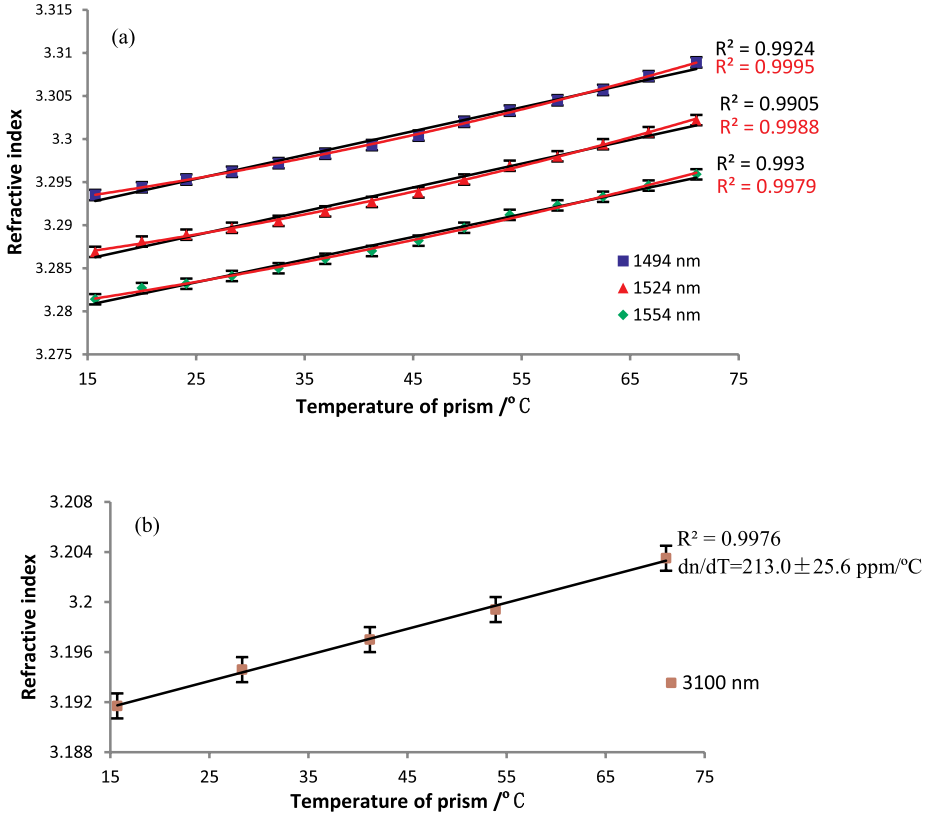

Fig. 8. The refractive index of $Ge_{16}As_{24}Se_{15.5}Te_{44.5}$ at. % prism with temperature at the wavelengths of: (a) 1494, 1524, 1554 nm with linear and quadratic fits applied to the data points, and (b) 3100 nm with a linear fit applied to the data points.

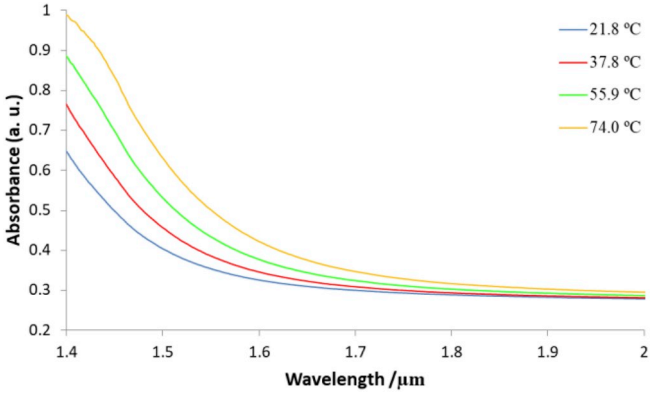

Fig. 9. The FTIR absorption spectra of bulk $Ge_{16}As_{24}Se_{15.5}Te_{44.5}$ at. % glass sample at sample temperatures of 21.8 °C, 37.8 °C, 55.9 °C and 74.0 °C showing the redshift of the optical bandgap.

evaporated As_2Se_3 at. Ratio thin film to a stated 'accuracy' (precision) of better than 3%. However, since the original dispersive model in this method (a Cauchy equation) cannot encompass the entire chalcogenide-glass transparent window (0.4–33 μm) [17], this method becomes invalid when applied to determine the refractive index of chalcogenide glasses in the MIR region.

In order to extend this method into the MIR spectral region (our measurements are over the wavelength range from 2 to 25 μm), the method was modified by us by using a two-term Sellmeier equation instead of the Cauchy equation as the dispersive equation [23,24]. A vacuum hot-pressing technique was used to fabricate chalcogenide glass thin films of 20 μm or 25 μm target thickness from fibers [23,24]. The characteristic interference fringes in the spectral transmission of these thin films, one at normal incidence and another at oblique incidence, were obtained over the wavelength range from 2 to 25 μm by FTIR (Fourier transform infrared) spectroscopy. This improved method was successfully applied to determine the refractive index of $As_{40}Se_{60}$ at. % and $Ge_{16}As_{24}Se_{15.5}Te_{44.5}$ at. % thin films over the wavelength range from 2 μm to 25 μm to an accuracy of better than 99.6% [23,24]. The average thicknesses of the non-uniform thin films were also determined by the improved Swanepoel method presented. Repeated measurements showed that the refractive index dispersion is determined by the improved method with a standard deviation of precision less than 0.002 for the $As_{40}Se_{60}$ at. % thin films and $Ge_{16}As_{24}Se_{15.5}Te_{44.5}$ at. % thin films over the wavelength range from 3 to 23 μm.

Several applications, such as biomedical sensing [43], call for the use of glasses with small compositional (and hence refractive index) difference to form chalcogenide glass optical fibers having a low NA (numerical aperture). In a recent extension to the work of [23], an unstructured fiber of the core composition ($Ge_{20}Sb_{10}Se_{70}$ at. %) was hot-pressed together with an unstructured fiber of the cladding composition ($Ge_{20}Sb_{10}Se_{67}S_3$ at. %) to form a two-composition thin film, with the advantages of the two glasses having the same thermal history and post-fiber processing [96]. The normal-incidence transmission spectra, spanning the wavelength region 15–27 μm and obtained at different spatial regions of the $Ge_{20}Sb_{10}Se_{70}$ at. %/$Ge_{20}Sb_{10}Se_{67}S_3$ at. % two-composition thin film are shown in Fig. 10. As the incoming beam shifted from the $Ge_{20}Sb_{10}Se_{70}$ at. % part to the $Ge_{20}Sb_{10}Se_{67}S_3$ at. % part of the thin film, which is from points 1 to 6 in Fig. 10, the extrema of each transmission spectrum shifted gradually to shorter wavelength. Since the thickness variation across the thin film was typically less than 0.05 μm, the shift of the extrema indicated that the $Ge_{20}Sb_{10}Se_{70}$ at. % thin film had a higher refractive index than the $Ge_{20}Sb_{10}Se_{67}S_3$ at. % thin film. The refractive indices and thicknesses of $Ge_{20}Sb_{10}Se_{70}$ at. % and $Ge_{20}Sb_{10}Se_{67}S_3$ at. % of the two-composition thin film were obtained using the improved Swanepoel method. Over the wavelength range 3–25 μm, the refractive index could be determined with a standard deviation of precision < 0.002 and the refractive index contrast could be determined with an measurement precision error of ± 0.0005. The NA of a SIF (step index fiber) comprising of a $Ge_{20}Sb_{10}Se_{70}$ at. % core and $Ge_{20}Sb_{10}Se_{67}S_3$ at. % cladding was determined from this technique with an error of ± 0.011, compared to the value of SIF NA from the prism minimum deviation method, on samples made from exactly the same two glass melts. In Ref. [96], it was reported that 3 at. % S replacing Se pro rata in the $Ge_{20}Sb_{10}Se_{70}$ at. % glass system (to formulate the cladding glass composition relative to the core glass composition) blue-shifted the NIR optical bandgap and MIR fundamental vibrational absorption bands, lowered the refractive index by 0.013 at a wavelength of 3.1 μm and by 0.012 at a wavelength of 6.45 μm, and moved the zero dispersion wavelength to a shorter wavelength: 6.3 to 6.1 μm.

5.2. A simple method to determine the small refractive index contrast

A fast and simple method was developed to compare the refractive index contrast of the two chalcogenide glass compositions ($Ge_{20}Sb_{10}Se_{70}$ at. %/$Ge_{20}Sb_{10}Se_{67}S_3$ at. %) (core/cladding glasses) comprising the thin film (illustrated in Fig. 10(a)) by using the normal-incidence transmission spectra only. The basic theory of this method is described in detail in Refs. [24,96]. When using the spectra at point 2 and point 5 in Fig. 10(a), the refractive contrast could be determined over the wavelength range from 2 to 25 μm with a measurement precision error of less than 0.0020 due to a typical thickness variation of < 0.05 μm in the two-composition thin film. It is expected that the thickness variation across a two-composition thin film can be further reduced by increasing the hot-pressing duration, by increasing the maximum pressing pressure applied and hot-pressing at a lower viscosity (higher temperature). An error of less than 0.0005 in determining the refractive index contrast can be obtained when the thickness variation across the thin film is controlled to be less than 0.01 μm.

5.3. A novel method to determine the continuous thermo-optic coefficient

In section 4.4, the thermo-optic coefficients of the chalcogenide glasses ($As_{40}Se_{60}$ at. % and $Ge_{16}As_{24}Se_{15.5}Te_{44.5}$ at. %) were determined using the prism minimum deviation method with a measurement precision error of less than ± 15.6 ppm/°C when using the tunable laser diode and with a measurement precision error of less than ± 25.6 ppm/°C when using the ICL. Due to the current limitation of available MIR beam sources, the *dn/dT* data at many interesting wavelengths in the MIR region are difficult to obtain using a prism-based approach [94].

An improved Swanepoel was successfully developed, which can determine the refractive index of chalcogenide glasses across the MIR region, using a FTIR spectrometer, to within 0.4% of the benchmark value obtained using the minimum deviation method [23]. Unlike the minimum deviation method, this technique produces a continuous refractive index curve over the wavelength range from 2 to 25 μm. The refractive indices of chalcogenide glasses in the MIR region can be determined using the improved Swanepoel method described in Section 5.1 of this mini review. However, since the measurement range of temperature was from 20 °C to 80 °C, a ± 0.002 difference in refractive index can lead to an estimate of the difference between the calculated and true values of *dn/dT* of ± 67 ppm/°C in the worst case. Therefore, a more accurate method is required to determine the thermo-optic coefficient of chalcogenide glasses.

To address this need, a novel method was successfully developed to determine the continuous thermo-optic coefficient of chalcogenide glasses over the wavelength range from 2 to 20 μm based on FTIR transmission spectra measured at different temperatures and the measured thermal expansion coefficient [24,97]. It was shown that this method can successfully determine the thermo-optic coefficient of the chalcogenide glass thin films ($Ge_{16}As_{24}Se_{15.5}Te_{44.5}$ at. % and $As_{40}Se_{60}$

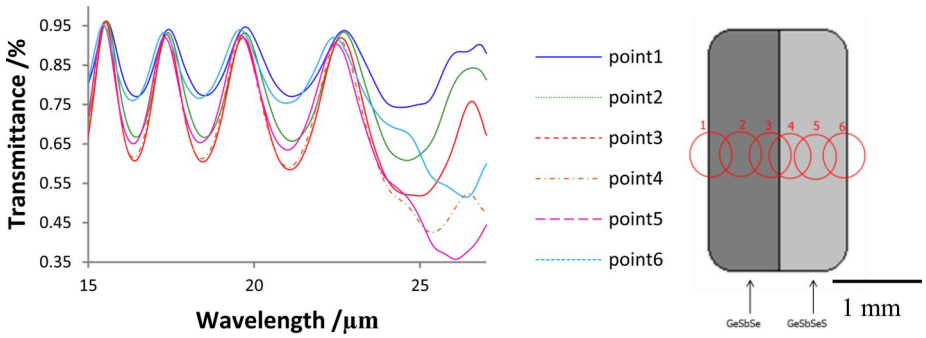

Fig. 10. (a) The transmission spectra at different locations (shown schematically in (b)) of a two-composition ($Ge_{20}Sb_{10}Se_{70}$ at. %/$Ge_{20}Sb_{10}Se_{67}S_3$ at. %) (core/cladding glasses) thin film. Points 2 and 5 were most representative of the core glass and cladding glass, respectively, without edge or interfacial effects.

at. %) over the wavelength range from 2 to 20 μm with a measurement precision error of less than ± 7.5 ppm/°C. Compared to both the minimum deviation method and the improved Swanepoel method, the proposed method was shown to provide a much lower error.

In this mini review, this novel method was used to determine the thermo-optic coefficient of a hot-pressed chalcogenide glass thin film with negative dn/dT ($As_{39}S_{61}$ at. %). The $As_{39}S_{61}$ at. % glass was synthesized at the Naval Research Laboratory, USA, and then subsequently drawn into fiber from which thin film samples were pressed at The University of Nottingham, UK. The thermo-optic coefficient was successfully determined using the novel method, as shown in Fig. 11, with a measurement precision error of less than ± 7.0 ppm/°C. The error analysis of this technique is described in Refs. [24,97]. The thermo-optic coefficients obtained using the prism minimum deviation refractometry were within the error of the results got using the present method. Any difference in dn/dT between these two techniques might also be attributed to the difference thermal history between a hot-pressed thin film and a chalcogenide glass prism.

Fig. 11 also shows that the dn/dT of $As_{39}S_{61}$ at. % decreases with increasing wavelength in the shorter wavelength region, which is due to the red shift of the optical band gap with temperature. At wavelengths above 10 μm, the dn/dT starts to increase with wavelength as shown in Fig. 11. This is attributed to the red shift of the fundamental multi-phonon absorption band with temperature.

6. Conclusions

In this paper, we have provided a mini review of three groups of methods: a prism minimum deviation method, spectroscopic ellipsometry and thin film FTIR (Fourier transform infrared) spectrometric methods, used by us to determine the refractive indices and thermo-optic coefficients of chalcogenide glasses at mid-infrared wavelengths; we hope these will be of use to the community. Although spectroscopic ellipsometry is probably the most popular technique for measuring refractive index dispersion in the mid-infrared region, it has disadvantages of high cost, requiring correct mathematical parameter fitting and being sensitive to surface effects. In contrast, the lower cost techniques employed here have been proved to yield sufficiently precise refractive index dispersions and thermo-optic coefficients of chalcogenide glasses.

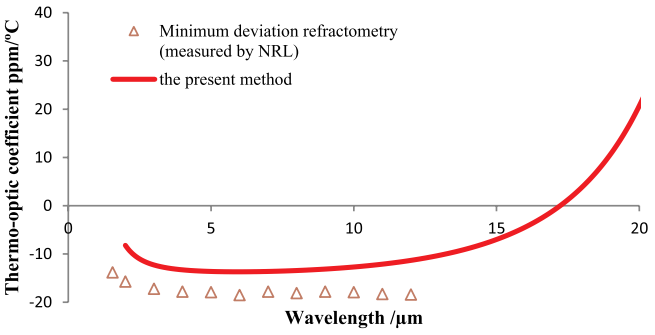

Fig. 11. The thermo-optic coefficients of the hot-pressed $As_{39}S_{61}$ at. % thin films obtained using the method presented here (solid line) compared to those obtained using the minimum deviation refractometry (triangles).

With the advantages of high accuracy and insensitivity to any oxide surface layer, prism methods, including the traditional minimum deviation method, minimum deviation refractometry (and prism coupling – not presented here) have been widely used to determine the refractive indices and thermo-optic coefficients of chalcogenide glasses. The current limitation of coherent beam sources means that it is not at present possible to make continuous refractive index dispersion measurements using this technique; the use of supercontinuum sources may in the future overcome this limitation. The refractive indices and thermo-optic coefficients of chalcogenide glasses obtained using our experimental prism minimum deviation set-up were presented here; the method requires production of prims with flat adjacent surfaces and controlled apex angle. It was shown that, with good beam sources, the refractive index can be determined with a standard deviation of precision < 0.001 and the thermo-optic coefficient can be obtained with a measurement precision error of < ± 15.6 ppm/°C.

In detail, the refractive indices and extinction coefficients of bulk prisms of $Ge_{16}As_{24}Se_{15.5}Te_{44.5}$, $As_{40}Se_{60}$, $Ge_{10}As_{23.4}Se_{66.6}$, $Ge_{16.5}As_{16}Ga_3Se_{64.5}$ and Pr^{3+} doped $Ge_{16}As_{21}Ga_1Se_{62}$ at. % glasses using the minimum deviation method have been presented. By fitting the data points to different refractive index models, a two-term Sellmeier equation was demonstrated to be the most suitable for describing the refractive index dispersion of chalcogenide glasses in the MIR region.

A Swanepoel method, improved for measurements on chalcogenide glass samples at mid-infrared wavelengths by using a two-term Sellmeier equation of refractive index dispersion to replace the Cauchy equation of Swanepoel's original paper, was developed to determine the refractive index of the chalcogenide thin films (again, in detail of: $Ge_{16}As_{24}Se_{15.5}Te_{44.5}$, $As_{40}Se_{60}$, $Ge_{10}As_{23.4}Se_{66.6}$, $Ge_{16.5}As_{16}Ga_3Se_{64.5}$ and Pr^{3+} doped $Ge_{16}As_{21}Ga_1Se_{62}$ at. % glasses) at mid-infrared wavelengths using FTIR transmission spectra. This technique has the advantages of wide-wavelength-range characterization, insensitivity to surface defects and speed of measurement once thin-film samples have been prepared. However, currently, this technique can only determine the refractive index with a standard deviation of precision of less than 0.002, which led to a large error in determining the thermo-optic coefficient. Therefore a novel method was successfully developed here to determine the continuous thermo-optic coefficient of chalcogenide glasses over the wavelength range from 2 to 20 μm with a measurement precision error of less than 7.5 ppm/°C; this was based on FTIR transmission spectra measured at different temperatures and the measured thermal expansion coefficient, and which also allowed calculation of the thermal polarizability coefficient.

Declaration of competing interest

The authors declare that they have no known competing financial interests or personal relationships that could have appeared to influence the work reported in this paper.

Acknowledgements

The authors are grateful to Mr Wojciech Rozwadowski for his help with the design of the temperature-controlled sample holder used for thermo-optic coefficient measurements. We thank Dr J. Meyer of the Naval Research Laboratory, United States of America, for supplying the 3.1 μm ICL and Chromacity Ltd, UK, for loaning us the 6.45 μm OPO (optical parametric oscillator) that were used for the prism measurements reported in this work.

References

[1] A.B. Seddon, Chalcogenide glasses: a review of their preparation, properties and application, J. Non-Cryst. Solids 184 (1995) 44–50.
[2] A. Zakery, S.R. Elliott, Optical properties and applications of chalcogenide glasses: a review, J. Non-Cryst. Solids 330 (2003) 1–12.
[3] J.S. Sanghera, I.D. Aggarwal, Active and passive chalcogenide glass optical fibers for IR applications: a review, J. Non-Cryst. Solids 256 (1999) 6–16.
[4] B. Cole, L.B. Shaw, P.C. Pureza, R. Mossadegh, J.S. Sanghera, I.D. Aggarwal, Rare-earth doped selenide glasses and fibers for active applications in the near and mid-IR, J. Non-Cryst. Solids 256 (1999) 253–259.
[5] J.S. Sanghera, L.B. Shaw, I.D. Aggarwal, Chalcogenide glass-fiber-based mid-IR sources and applications, IEEE J. Sel. Top. Quant. 1 (2009) 114–119.
[6] Z. Tang, D. Furniss, M. Fay, H. Sakr, L. Sójka, N. Neate, N. Weston, S. Sujecki, T.M. Benson, A.B. Seddon, Mid-infrared photoluminescence in small-core fiber of praseodymium-ion doped selenide-based chalcogenide glass, Opt. Mater. Express 5 (2015) 870–886.
[7] M.C. Falconi, G. Palma, F. Starecki, V. Nazabal, J. Troles, J.L. Adam, S. Taccheo, M. Ferrari, F. Prudenzano, Dysprosium-doped chalcogenide master oscillator power amplifier (MOPA) for mid-IR emission, J. Light. Technol. 3 (5) (2017) 265–273.
[8] A.B. Seddon, W.J. Pan, D. Furniss, C.A. Miller, H. Rowe, D. Zhang, E. McBrearty, Y. Zhang, A. Loni, P. Sewell, T.M. Benson, Fine embossing of chalcogenide glasses–a new fabrication route for photonic integrated circuits, J. Non-Cryst. Solids 352 (2006) 2515–2520.
[9] N.S. Abdel-Moneim, C.J. Mellor, T.M. Benson, D. Furniss, A.B. Seddon, Fabrication of stable, low optical loss rib-waveguides via embossing of sputtered chalcogenide glass-film on glass-chip, Opt. Quant. Electron. 47 (2015) 351–361.
[10] F. Starecki, S. Morais, R. Chahal, C. Boussard-Plédal, B. Bureau, F. Palencia, C. Lecoutre, Y. Garrabos, S. Marre, V. Nazabal, IR emitting Dy^{3+} doped chalcogenide fibers for in situ CO_2 monitoring in high pressure microsystems, Int. J. of Greenhouse Gas Control 55 (2016) 36–41.
[11] J. Ari, F. Starecki, C. Boussard-Plédel, Y. Ledemi, Y. Messaddeq, J.-L. Doualan, A. Braud, B. Bureau, V. Nazabal, Co-doped Dy^{3+} and Pr^{3+} $Ga_5Ge_{20}Sb_{10}S_{65}$ fibers for mid-infrared broad emission, Opt. Lett. 43 (2018) 2893–2896.
[12] L. Sojka, Z. Tang, D. Jayasuriya, M. Shen, D. Furniss, E. Barney, T.M. Benson, A.B. Seddon, S. Sujecki, Ultra-broadband mid-infrared emission from Pr^{3+}/Dy^{3+} co-doped selenide-chalcogenide glass fiber spectrally shaped by varying the pumping arrangement, Opt. Mater. Express 9 (2019) 2291–2306.
[13] R.R. Gattass, L.B. Shaw, V.Q. Nguyen, P.C. Pureza, I.D. Aggarwal, J.S. Sanghera, All-fiber chalcogenide-based mid-infrared supercontinuum source, Opt. Fiber Technol. 18 (2012) 345–348.
[14] C.R. Petersen, U. Møller, I. Kubat, B. Zhou, S. Dupont, J. Ramsay, T. Benson, S. Sujecki, N. Abdel-Moneim, Z. Tang, D. Furniss, Mid-infrared supercontinuum covering the 1.4-13.3 mum molecular fingerprint region using ultra-high NA chalcogenide step-index fibre, Nat. Photonics 8 (2014) 830–834.
[15] J. Hu, C.R. Menyuk, C. Wei, L.B. Shaw, J.S. Sanghera, I.D. Aggarwal, Highly efficient cascaded amplification using Pr^{3+}-doped mid-infrared chalcogenide fiber amplifiers, Opt. Lett. 40 (2015) 3687–3690.
[16] E.A. Anashkina, Design and Numerical Modeling of Broadband Mid-IR rare-earth doped chalcogenide fiber amplifiers, IEEE Photonics Technol. Lett. 30 (2018) 1190–1193.
[17] M. Shen, D. Furniss, Z. Tang, E. Barny, L. Sojka, S. Sujecki, T.M. Benson, A.B. Seddon, Modeling of resonantly pumped mid-infrared Pr^{3+}-doped chalcogenide fiber amplifier with different pumping schemes, Opt. Express 26 (2018) 23641–23660.
[18] J. Orava, T. Kohoutek, T. Wagner, Z. Cerna, M. Vlcek, L. Benes, B. Frumarova, M. Frumar, Optical and structural properties of Ge–Se bulk glasses and Ag–Ge–Se thin films, J. Non-Cryst. Solids 355 (2009) 1951–1954.
[19] H.A. Qiao, N.C. Anheier, J.D. Musgrave, K. Richardson, D.W. Hewak, Measurement of chalcogenide glass optical dispersion using a mid-infrared prism coupler, Window and Dome Technologies and Materials XII 8016, International Society for Optics and Photonics, 2011, p. 80160F.
[20] H.G. Dantanarayana, N. Abdel-Moneim, Z. Tang, L. Sojka, S. Sujecki, D. Furniss, A.B. Seddon, I. Kubat, O. Bang, T.M. Benson, Refractive index dispersion of chalcogenide glasses for ultra-high numerical-aperture fiber for mid-infrared supercontinuum generation, Opt. Mater. Express 4 (2014) 1444–1455.
[21] B. Gleason, K. Richardson, L. Sisken, C. Smith, Refractive index and thermo-optic coefficients of Ge-As-Se chalcogenide glasses, Int. J. Appl. Glass Sci. 7 (2016) 374–383.
[22] Y. Wang, S. Qi, Z. Yang, R. Wang, A. Yang, P. Lucas, Composition dependences of refractive index and thermo-optic coefficient in Ge-As-Se chalcogenide glasses, J. Non-Cryst. Solids 459 (2017) 88–93.
[23] Y. Fang, D. Jayasuriya, D. Furniss, Z.Q. Tang, C. Markos, S. Sujecki, A.B. Seddon, T.M. Benson, Determining the refractive index dispersion and thickness of hot-pressed chalcogenide thin films from an improved Swanepoel method, Opt. Quant. Electron. 49 (2017) 237.
[24] Y. Fang, Assessing the Optical Properties of Chalcogenide Glasses and Fibres: towards the Development of New Light Sources, PhD Thesis, University of Nottingham, UK, 2019.
[25] Amorphous material Inc, AMTIR-1 Information, (2013).
[26] Amorphous material Inc, AMTIR-2 Information, (2013).
[27] Amorphous material Inc, AMTIR-3 Information, (2013).
[28] Amorphous material Inc, AMTIR-4 Information, (2013).
[29] Amorphous material Inc, AMTIR-5 Information, (2013).
[30] Amorphous material Inc, AMTIR-6 Information, (2013).
[31] Amorphous material Inc, C1 Information, (2013).
[32] Schott Glass Inc, Schott Infrared Chalcogenide Glass – IRG22, (2013).
[33] Schott Glass Inc, Schott Infrared Chalcogenide Glass – IRG23, (2013).
[34] Schott Glass Inc, Schott Infrared Chalcogenide Glass – IRG24, (2013).
[35] Schott Glass Inc, Schott Infrared Chalcogenide Glass – IRG25, (2013).
[36] Schott Glass Inc, Schott Infrared Chalcogenide Glass – IRG26, (2013).
[37] Schott Glass Inc, Schott Infrared Chalcogenide Glass – IRG27, (2013).
[38] Schott Glass Inc, Schott Infrared Chalcogenide Glass – IRG26, (2013).
[39] Schott Glass Inc, Schott Infrared Chalcogenide Glass – IRG26, (2013).
[40] E.D. Palik (Ed.), Handbook of Optical Constants of Solids, Academic Press, Orlando, 1985.
[41] Z. Tang, D. Furniss, N.C. Neate, T.M. Benson, A.B. Seddon, Low gallium-content, dysprosium III-doped, Ge-As-Ga-Se chalcogenide glasses for active mid-infrared fiber optics, J. Am. Ceram. Soc. 102 (2019) 195–206.
[42] H. Sakr, Z. Tang, D. Furniss, L. Sojka, S. Sujecki, T.M. Benson, A.B. Seddon, Promising emission behavior in Pr^{3+}/In selenide-chalcogenide-glass small-core step index fiber (SIF), Opt. Mater. 67 (2017) 98–107.
[43] H. Parnell, Towards a Ge-Sb-Se/S Hyperspectral Imaging Probe for Early Cancer Diagnosis, PhD thesis University of Nottingham, UK, 2018.
[44] H. Parnell, D. Furniss, Z. Tang, N.C. Neate, T.M. Benson, A.B. Seddon, Compositional dependence of crystallization in Ge–Sb–Se glasses relevant to optical fiber making, J. Am. Ceram. Soc. 101 (2018) 208–219.
[45] D. Jayasuriya, Towards Mid-infrared Fibre-Optic Device and Systems for Sensing, Mapping and Imaging, PhD thesis University of Nottingham, UK, 2018.
[46] R. Swanepoel, Determining refractive index and thickness of thin films from wavelength measurements only, J. Opt. Soc. Am. A 2 (1985) 1339–1343.
[47] E. Collet, Digital refractometry, Optics Comms. 63 (1987) 217–224.
[48] E. Marquez, J.M. González-Leal, R. Prieto-Alcón, M. Vlcek, A. Stronski, T. Wagner, D. Minkov, Optical characterization of thermally evaporated thin films of $As_{40}S_{40}Se_{20}$ chalcogenide glass by reflectance measurements, Appl. Phys. A 67 (1998) 371–378.
[49] D. Poelman, P.F. Smet, Methods for the determination of the optical constants of thin films from single transmission measurements: a critical review, J. Phys. D Appl. Phys. 36 (2003) 1850–1857.
[50] N. Carlie, L. Petit, J.D. Musgraves, K. Richardson, N.C. Anheier Jr., H.A. Qiao, B. Bernacki, M.C. Phillips, Measurement of the refractive index dispersion of As_2Se_3 bulk glass and thin films prior to and after laser irradiation and annealing using prism coupling in the near-and mid-infrared spectral range, Rev. Sci. Instrum. 82 (2011) 053103-053103.
[51] J.M. Laniel, J.M. Ménard, K. Turcotte, A. Villeneuve, R. Vallée, C. Lopez, K.A. Richardson, Refractive index measurements of planar chalcogenide thin film, J. Non-Cryst. Solids 1 (2003) 183–191.
[52] Y. Fang, L. Sojka, D. Jayasuriya, D. Furniss, Z.Q. Tang, C. Markos, S. Sujecki, A.B. Seddon, T.M. Benson, Characterising refractive index dispersion in chalcogenide glasses, Proc. 18th International Conference on Transparent Optical Networks, IEEE, 2016.
[53] I. Vurgaftman, R. Weih, M. Kamp, J.R. Meyer, C.L. Canedy, C.S. Kim, M. Kim, W.W. Bewley, C.D. Merritt, J. Abell, S. Höfling, Interband cascade lasers, J. Phys. D 48 (2015) 123001.
[54] M. Kim, C.S. Kim, C.l. Canedy, W.W. Bewley, C.D. Merritt, I. Vurgaftman, J.R. Meyer, Interband cascade lasers with sidewall corrugations for enhanced brightness, SPIE Proceedings Volume 10939, Novel In-Plane Semiconductor Lasers XVIII, 2019 109390X https://doi.org/10.1117/12.2508703.
[55] J. Liu, Photonic Devices, Cambridge University Press, 2005.
[56] G.E. Jellison Jr., F.A. Modine, Parameterization of the optical functions of amorphous materials in the interband region, Appl. Phys. Lett. 69 (1996) 371–373.
[57] G.E. Jellison Jr., F.A. Modine, Erratum: parameterization of the optical functions of amorphous materials in the interband region, Appl. Phys. Lett. 69 (1996) 2137.
[58] F.A. Jenkins, H.E. White, Fundamentals of Optics, Tata McGraw-Hill Education, 1937.
[59] H.G. Dantanarayana, Application of TLM for Optical Microresonators, PhD thesis University of Nottingham, UK, 2012.
[60] W. Sellmeier, Zur Erkarung der abnormen Farbenfolge im Spectrum einiger, Substanzen Annalen der Physik und Chemie 210 (1871) 272–282.
[61] G. Beadie, E. Stover, D. Gibson, Temperature-dependent dispersion fitting for a

recent infrared glass catalog, Proc. SPIE 10998 (2019) 03.
[62] M. Herzberger, C.D. Salzberg, Refractive indices of infrared optical materials and color correction of infrared lenses, J. Opt. Soc. Am. 52 (1962) 420–427.
[63] A.F.J. Levi, Essential Classical Mechanics for Device Physics, Morgan & Claypool Publishers, 2016.
[64] J. Tauc, R. Grigorovici, A. Vancu, Optical properties and electronic structure of amorphous germanium, Phys. Status Solidi 15 (1966) 627–637.
[65] F. Wooton, Optical Properties of Solids, Academic Press, New York, 1972.
[66] J.I. Pankove, Hydrogenated Amorphous Silicon: Device Applications, Academic Press, London, 1984.
[67] A.S. Ferlauto, G.M. Ferreira, J.M. Pearce, C.R. Wronski, R.W. Collins, X. Deng, G. Ganguly, Analytical model for the optical functions of amorphous semiconductors from the near-infrared to ultraviolet: applications in thin film photovoltaics, J. Appl. Phys. 92 (2002) 2424–2436.
[68] P. Němec, M. Olivier, E. Baudet, A. Kalendova, P. Benda, V. Nazabal, Optical properties of $(GeSe_2)_{100-x}(Sb_2Se_3)_x$ glasses in near-and middle-infrared spectral regions, Mater. Res. Bull. 51 (2014) 176–179.
[69] P. Hawlová, F. Verger, V. Nazabal, R. Boidin, P. Němec, Accurate determination of optical functions of Ge–As–Te glasses via spectroscopic ellipsometry, J. Am. Ceram. Soc. 97 (2014) 3044–3047.
[70] J. Orava, J. Šik, T. Wagner, M. Frumar, Optical properties of $As_{33}S_{67-x}Se_x$ bulk glasses studied by spectroscopic ellipsometry, J. Appl. Phys. 103 (2008) 083512.
[71] P. Němec, M. Frumar, Photoinduced phenomena in As_4Se_3 amorphous thin films prepared by pulsed laser deposition, Thin Solid Films 516 (2008) 8377–8380.
[72] R. Todorov, A. Paneva, K. Petkov, Optical characterization of thin chalcogenide films by multiple-angle-of-incidence ellipsometry, Thin Solid Films 518 (2010) 3280–3288.
[73] C.C. Lee, S.L. Ku, Study on the optical property and crystallinity of $Ge_{90}Te_{10}$ films deposited by electron beam evaporation, Thin Solid Films 519 (2011) 1794–1797.
[74] G.A.M. Amin, Studies on $In_x(As_2Se_3)_{1-x}$ thin films using variable angle spectroscopic ellipsometry (VASE), Mater. Sci.-Poland 33 (2015) 501–507.
[75] S. Guo, X.J. Ding, J.Z. Zhang, Z.G. Hu, X.L. Ji, L.C. Wu, Z.T. Song, J.H. Chu, Intrinsic evolutions of dielectric function and electronic transition in tungsten doping $Ge_2Sb_2Te_5$ phase change films discovered by ellipsometry at elevated temperatures, Appl. Phys. Lett. 106 (2015) 052105.
[76] A. Velea, G. Socol, M. Popescu, A.C. Galca, In-situ characterization of the optical and electronic properties in GeTe and GaSb thin films, J. Appl. Phys. 118 (2015) 135712.
[77] F. Abdel-Wahab, A. Merazga, M.S. Rasheedy, A.A. Montaser, Optical characterization of the annealing effect on $Ge_5Te_{20}Se_{75}$ thin films by variable angle of-incidence spectroscopic ellipsometry, Optik 127 (2016) 3871–3877.
[78] N.N. Wei, Z. Yang, H.B. Pan, F. Zhang, Y.X. Liu, R.P. Wang, X. Shen, S.X. Dai, Q.H. Nie, Variable angle spectroscopic ellipsometry and its applications in determining optical constants of chalcogenide glasses in infrared, Chin. Phys. B 27 (2018) 067802.
[79] L.H. Malitson, Interspecimen comparison of the refractive index of fused silica, J. Opt. Soc. Am. A 55 (1965) 1917–1983.
[80] L.W. Tilton, Prism size and orientation in minimum-deviation refractometry, Nat. Bur. Stand. J. Research 6 (1931) 59–76.
[81] D. Tentori, J.R. Lerma, Refractometry by minimum deviation: accuracy analysis, Opt. Eng. 29 (1990) 160–168 1990.
[82] A.K. Walton, T.S. Moss, Determination of refractive index and correction to effective electron mass in PbTe and PbSe, Proc. Phys. Soc. 81 (1963) 509.
[83] X.H. Zhang, Y. Guimond, Y. Bellec, Production of complex chalcogenide glass optics by molding for thermal imaging, J. Non-Cryst. Solids 326 (2003) 519–523.
[84] A.B. Seddon, M.J. Laine, Chalcogenide glasses for acousto-optic devices. II. As–Ge–Se systems, J. Non-Cryst. Solids 213 (1997) 168–173.
[85] E. Guillevic, X. Zhang, T. Pain, L. Calvez, J.L. Adam, J. Lucas, M. Guilloux-Viry, S. Ollivier, G. Gadret, Optimization of chalcogenide glass in the As–Se–S system for automotive applications, Opt. Mater. 31 (2009) 1688–1692.
[86] H.L. Ma, Y. Guimond, X.H. Zhang, J. Lucas, Ga–Ge–Sb–Se based glasses and influence of alkaline halide addition, J. Non-Cryst. Solids 256 (1999) 165–169.
[87] J. Novak, R. Pini, W.V. Moreshead, E. Stover, A. Symmons, Investigation of index of refraction changes in chalcogenide glasses during molding processes, Electro-Optical and Infrared Systems: Technology and Applications X 8896, International Society for Optics and Photonics, 2013, p. 889602.
[88] J. Novak, S. Novak, J. Huddleston, W. Moreshead, A. Symmons, E. Stover, Compositional dependence of properties and lens performance of As-Se chalcogenide glass, Advanced Optics for Defense Applications: UV through LWIR II, International Society for Optics and Photonics, 2017, p. 10181 101810Q.
[89] J. Novak, A. Symmons, S. Novak, E. Stover, Applicability of an annealing coefficient for precision glass molding of $As_{40}Se_{60}$, Advanced Optics for Defense Applications: UV through LWIR, International Society for Optics and Photonics, 2016, p. 9822 98220A.
[90] W. S Rodney, I.H. Malitson, T.A. King, Refractive index of arsenic trisulfide, J. Opt. Soc. Am. 48 (1958) 633–636.
[91] J. Nishii, S. Morimoto, I. Inagawa, R. Iizuka, T. Yamashita, T. Yamagishi, Recent advances and trends in chalcogenide glass fiber technology: a review, J. Non-Cryst. Solids 140 (1992) 199–208.
[92] J.D. Musgraves, S. Danto, K. Richardson, Thermal properties of chalcogenide glasses, Chalcogenide Glasses (2014) 82–112.
[93] L. Prod'homme, A new approach to the thermal change in the refractive index of glasses, Phys. Chem. Glasses 1 (1960) 119–122.
[94] A.R. Hilton, C.E. Jones, The thermal change in the nondispersive infrared refractive index of optical materials, Appl. Optic. 6 (1967) 1513–1517.
[95] C. Corrales, J.B. Ramírez-Malo, J. Fernández-Peña, P. Villares, R. Swanepoel, E. Márquez, Determining the refractive index and average thickness of AsSe semiconducting glass films from wavelength measurements only, Appl. Optic. 34 (1995) 7907–7913.
[96] Y. Fang, D. Furniss, D. Jayasuriya, H. Parnell, R. Crane, Z.Q. Tang, E. Barney, C.L. Canedy, C.S. Kim, M. Kim, C.D. Merritt, W.W. Bewley, I. Vurgaftman, J.R. Meyer, A.B. Seddon, T.M. Benson, Determining small refractive index contrast in chalcogenide-glass pairs at mid-infrared wavelengths, Opt. Mater. Express 9 (2019) 2022–2036.
[97] Y. Fang, D. Furniss, D. Jayasuriya, H. Parnell, Z. Tang, A.B. Seddon, T. M Benson, Determining the Continuous Thermo-Optic Coefficients of Chalcogenide Glass Thin Films in the MIR Region Using FTIR Transmission Spectra, submitted for publication, 2019.